PHYSICAL REVIEW B **90**, 184424 (2014)

# Ferroelectricity in spiral short-range-ordered magnetic state of spinel $MnCr_2O_4$: Significance of topological frustration and magnetoelastic coupling

K. Dey, S. Majumdar, and S. Giri[*]

*Department of Solid State Physics, Indian Association for the Cultivation of Science, Jadavpur, Kolkata 700032, India*

(Received 15 September 2014; revised manuscript received 30 October 2014; published 21 November 2014)

We report the appearance of ferroelectricity below $T_S = 18$ K, at which short-ranged spiral spin orders, suggesting that $MnCr_2O_4$ is an improper multiferroic material. Linear heat capacity data and zero-field-cooled memory effect verify reentrant spin-glass-like state below $T_S$. Synchrotron x-ray diffraction studies confirm significant magnetoelastic coupling at long-range ferrimagnetic order ($T_N = 42$ K) and at $T_S$. We argue that the release of topological spin frustration, produced due to pyrochlore structure of Cr sublattice, is manifested through the significant magnetoelastic effect at $T_N$ and $T_S$ and holds the key for spiral spin order driven ferroelectricity in $MnCr_2O_4$.

DOI: 10.1103/PhysRevB.90.184424 PACS number(s): 75.80.+q, 77.80.−e

## I. INTRODUCTION

Geometric frustration resulting from the underlying lattice geometry usually based on triangles or tetrahedra attracts considerable attention in magnetism due to occurrence of exotic phenomena; those are distinctly different from the usual magnetism involving conventional long-range magnetic order [1,2]. Most of the studies on geometrical frustration have been centered around the kagomé and pyrochlore based magnets in the past two decades. The $AB_2O_4$-type compound with spinel structure is one of the promising examples in this category where a $B$ site ion is surrounded by octahedral oxygen cages to form pyrochlore sublattice. Arrangements of corner sharing octahedra formed by pyrochlore $B$ sublattice are shown in Fig. 1(a). When $B$ sublattice is antiferromagnetically coupled, it produces significant magnetic frustration as depicted in Fig. 1(b) [3]. The $Cr^{3+}$ ions in $ACr_2O_4$ are observed to be antiferromagnetically coupled as recently found in the literature where geometrical frustration emerges due to $B$ site $Cr^{3+}$ ions and a nonmagnetic $A$ site ion does not directly influence the magnetic frustration [3–6]. Importantly, the Curie-Weiss temperatures ($\Theta_{CW}$) in $ACr_2O_4$ were found to be significantly higher than the long-range magnetic ordering temperature ($T_N$) for various $A$ ions. This provides large $\Theta_{CW}/T_N$ ratio as an indicative of the degree of magnetic frustration. For example, the values of $\Theta_{CW}$ were −32.0 K, −88.0 K, and −390.0 K, which were significantly higher than the values of $T_N$ as 6.0, 7.8, and 12.5 K for $HgCr_2O_4$ [4], $CdCr_2O_4$ [5], and $ZnCr_2O_4$ [6], respectively. When the $A$ site ion is magnetic, it partially releases the $B$ site frustration as $T_N$ shifts toward higher temperature [7–9]. The interplay between $A$ site and $B$ site magnetism usually provides a ground state comprised of spiral short-range magnetic order [7].

The cubic spinel $MnCr_2O_4$ crystallizes in $Fd\bar{3}m$ space group in a wide temperature range from 773 K down to room temperature. According to the spinel structure $Mn^{2+}$ and $Cr^{3+}$ reside at tetrahedral and octahedral sites, respectively, where corners of tetrahedra and octahedra are occupied by oxygen atoms [8]. $MnCr_2O_4$ orders ferrimagnetically at $T_N$ in the range 41–51 K, followed by a short-range spiral order at low temperature, $T_S = 14$–18 K [8,10–13]. Neutron diffraction [7,14,15] and NMR studies [16] confirm the coexistence of ferrimagnetic and spiral short-range-ordered components below $T_S$ suggesting this to be a consequence of delicate interplay between $A$ site and frustrated $B$ site magnetism, as also proposed from first-principle calculation [17]. Recently, local magnetoelectric effect arising from the noncentrosymmetric magnetic sites [18] and a weak magnetodielectric response [19] were reported for $MnCr_2O_4$, which are the preliminary factors of a multiferroic material. Direct observation of the spontaneous electric polarization either from ferroelectric hysteresis loop or pyroelectric current measurement could settle the issue on multiferroic orders.

Recent discovery of multiferroic order correlated to the frustration revives renewed attention in this field. Frustration leads to the intricate ground state and commonly incommensurate magnetic order is realized, for example, in $NiBr_2$ [20] and $Ni_3V_2O_8$ [21]. Thus magnetic frustration is a powerful source of "unconventional" magnetic orders, which can induce ferroelectricity. Analogous to that observed in $MnCr_2O_4$, the spiral magnetic order is realized as a consequence of strong magnetic frustration driven by the pyrochlore structure of Cr sublattice for $CoCr_2O_4$ [7]. Because of spiral magnetic order ferroelectricity (FE) was proposed in $CoCr_2O_4$ nearly one decade ago [22], although FE has not been identified for $MnCr_2O_4$ having similar magnetic ground state.

In this article we demonstrate the emergence of ferroelectric order below $\sim T_S$ associated with additional features. Intriguingly, ferroelectricity is observed in a re-entrant spin-glass (SG) state below $T_S$ as verified from zero-field-cooled memory effect and analysis of the heat capacity data. X-ray synchrotron diffraction studies over a wide temperature range, 10–300 K, further reveal significant magnetoelastic coupling at $T_N$ and $T_S$, although it does not show any signature of symmetry lowering at $T_N$ and $T_S$. We propose that release of topological frustration is manifested through the magnetoelastic consequences at $T_N$ and $T_S$. The magnetoelastic response and spiral magnetic order at $T_S$ are the coupled phenomena which are correlated with the occurrence of FE order, proposing that $MnCr_2O_4$ is a new improper multiferroic material.

## II. EXPERIMENTAL DETAILS

Polycrystalline specimen $MnCr_2O_4$ are prepared by solid state reaction [16]. Single phase chemical composition is

---

[*] Corresponding author: sspsg2@iacs.res.in

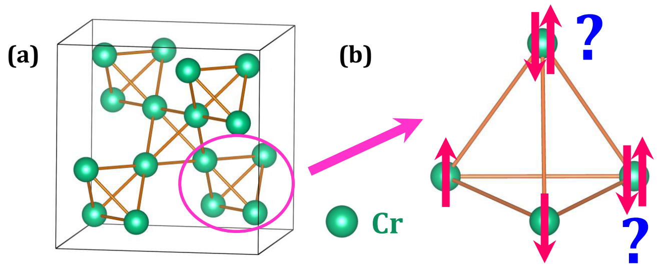

FIG. 1. (Color online) (a) Corner sharing tetrahedra formed by $Cr^{3+}$ sublattice in the spinel structure. (b) Example of antiferromagnetically coupled $Cr^{3+}$ sublattice forming a tetrahedron and demonstrating strong magnetic frustration.

confirmed by x-ray diffraction studies at room temperature recorded in a SEIFERT x-ray diffractometer (Model: XRAY3000P) using Cu $K\alpha$ radiation. This is further confirmed by the synchrotron x-ray diffraction studies measured partly at P07 beam line of Petra III, Hamburg, Germany at a wavelength of 0.1252 Å (99 keV) and partly at Indian beam line of Photon Factory, Japan in the temperature range 10–300 K. The synchrotron powder diffraction data are analyzed using Rietveld refinement with a commercially available software MAUD (materials analysis using diffraction) and further checked by FULLPROF software. Heat capacity ($C_P$) is measured using a homebuilt setup in the range 10–100 K [23]. Dielectric permittivity is measured on a compressed powder specimen in the range 6–300 K using an E4980A LCR meter (Agilent Technologies, USA) equipped with a cryogen-free cryocooler (JANIS, USA). The pyroelectric current ($I_p$) is recorded at a constant temperature sweep rate (4.0 K/min) using an electrometer (Keithley, model 6517B) and integrated with time for obtaining electric polarization ($P$). A poling electric field (150 kV/m) is applied during the cooling process and short circuited before the measurement of $I_p$ in the warming mode for the polarization measurement. Electrical contacts are fabricated using an air drying silver paint. The dc magnetization is measured by a commercial magnetometer of Quantum Design (MPMS, evercool).

## III. EXPERIMENTAL RESULTS AND DISCUSSIONS

Thermal variation of zero-field-cooled (ZFC) and field-cooled (FC) magnetization recorded at 100 Oe are displayed in Fig. 2(a). Inverse of susceptibility ($\chi^{-1}$) measured in ZFC protocol is shown in the inset of the figure. The linear fit using Curie-Weiss law is displayed by a straight line which provides paramagnetic moment, $\mu_{\text{eff}} \approx 1.99\mu_{\text{eff}}$ and Curie-Weiss temperature, $\Theta \approx -216$ K. The value of $\mu_{\text{eff}}$ is much smaller than that of the spin-only values for $Mn^{2+}$ ($5\mu_B$) and $Cr^{3+}$ ($3\mu_B$). This low $\mu_{\text{eff}}$ may appear due to consideration of $T$ range of magnetization below 300 K. Consideration of a paramagnetic region at much higher temperature may provide higher $\mu_{\text{eff}}$ value close to the theoretical value. However, this low $\mu_{\text{eff}}$ is consistent with the neutron diffraction study which also provided a much smaller ordered moment of $Mn^{2+}$ and $Cr^{3+}$ than the theoretical values [14,15]. The value of $\Theta$ is much larger than the ferrimagnetic (FIM) ordering temperature at 42 K ($T_N$) below which a sharp increase in both the ZFC and FC magnetization is observed, and ZFC-FC magnetization deviate from each other. A reasonably large value of $\Theta/T_N$ ratio (≈5.1) indicates magnetic frustration.

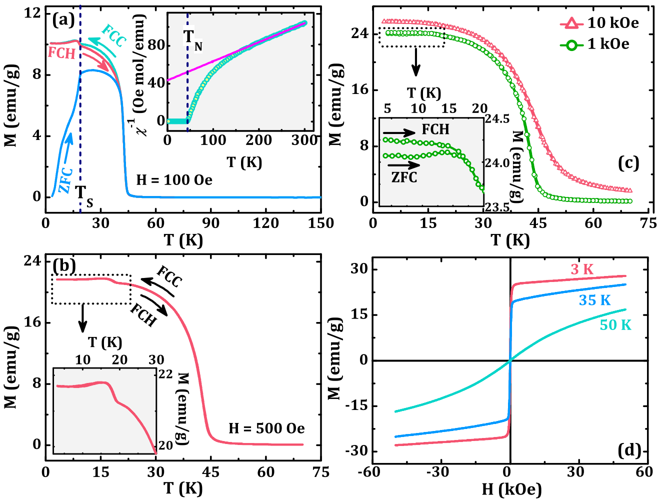

FIG. 2. (Color online) Thermal ($T$) variation of (a) ZFC-FC magnetization measured with 100 Oe. Thermal hysteresis between FCC and FCH is also shown. Inset of (a) displays inverse susceptibility ($\chi^{-1}$) plot with $T$. (b) Thermal hysteresis of magnetization disappears for measurement at 500 Oe. Inset of (b) highlights the low-$T$ FC magnetization. (c) $T$ variation of ZFC-FC magnetization measured at 1 and 10 kOe. Inset of (c) highlights deviation between ZFC and FC magnetization at low $T$. (d) Magnetic hysteresis loops at 3, 35, and 50 K.

Thermomagnetic irreversibility strongly depends on magnetic field ($H$) and decreases significantly with increasing $H$. It nearly disappears for $H \approx 10$ kOe as shown in Fig. 2(c). With decreasing temperature below $T_N$ a sharp fall is observed in the ZFC magnetization for $H = 0.1$ kOe around 18 K ($T_S$), below which an anomaly is observed for $H \approx 0.5$ kOe in the FC magnetization as shown in the inset of Fig. 2(b). The anomaly below $T_S$ slowly disappears for $H \approx 1$ kOe as evident in the inset of Fig. 2(c). A weak thermal hysteresis is observed in the FC magnetization for $H \approx 0.1$ kOe, which nearly disappears for $H \approx 0.5$ kOe as depicted in Fig. 2(b). Below $T_S$ development of a short-range spiral magnetic order has been proposed in addition to the long-range FIM order from neutron diffraction [7,14,15] and NMR studies [16]. Magnetic field dependent results suggest that the short-range spiral magnetic order is strongly influenced by the applied magnetic field. Magnetic hysteresis loops are measured at 3 ($<T_S$), 35 ($<T_N$), and 50 K ($>T_N$), as shown in Fig. 2(d). Magnetization curve provides low coercivity ∼90 Oe and displays a linear response for $H >\sim 1$ kOe at 3 and 35 K.

Heat capacity ($C_P$) as a function of temperature is depicted in Fig. 3(a) displaying apparent signatures of $T_N$ and $T_S$ at 42 and 18 K, respectively. Inset of Fig. 2(a) shows magnetic entropy ($C_{\text{mag}}$) displaying a linear dependence below ∼13.5 K above which it deviates from the linearity. $C_{\text{mag}}$ is determined by subtracting heat capacity data of spinel $MgAl_2O_4$ [24]. The linear temperature dependence of $C_{\text{mag}}$ is a characteristic signature of insulating [25] and metallic SGs [26].

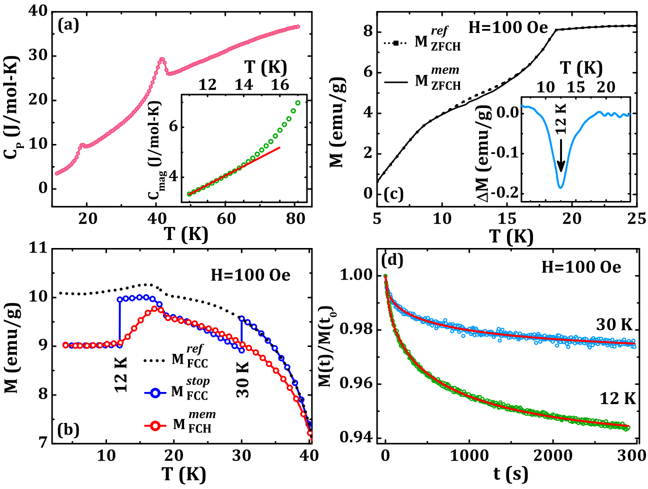

FIG. 3. (Color online) (a) $T$ variation heat capacity ($C_P$). Inset shows linear dependence of $C_{\mathrm{mag}}$ at low temperature where straight line guides the linear dependence. (b) Thermal variation of field-cooled (FC) magnetization in different modes. The field is cut off during temporary stops at 30 and 12 K. Memory effect is demonstrated by a step above 12 K and is absent at 30 K. (c) Thermal variation of ZFC magnetization defined as $M^{\mathrm{ref}}_{\mathrm{ZFCH}}$ (reference) and ZFC memory defined as $M^{\mathrm{mem}}_{\mathrm{ZFCH}}$. Inset shows thermal variation of difference plot ($\Delta M$) between $M^{\mathrm{ref}}_{\mathrm{ZFCH}}$ and $M^{\mathrm{mem}}_{\mathrm{ZFCH}}$, displaying convincing signature of memory effect at 12 K. (d) Time ($t$) dependence of $M$ at 12 and 30 K in zero field after cooling the sample in 100 Oe.

The frequency ($f$) dependence of ac susceptibility results is important for characterizing SG behavior which has already been investigated in polycrystalline $MnCr_2O_4$ [13]. The results were inconclusive because $f$ dependence could not be detected precisely for the analysis due to coexistence of SG and FIM states. We perform experiment on magnetic memory effect as described in the literature [27–29]. During cooling the sample is annealed at a wait temperature ($T_w$) and then cooled further down to the lowest $T$, after which the data are recorded in the warming cycle. Memory experiment is performed both in ZFC and FC protocols. For FC mode magnetic field is switched off during the aging or waiting ($t_w$) process. The $t_w$'s for FC and ZFC are 1 and 3 h, respectively. The $T_w$'s are fixed at 30 ($>T_S$) and 12 K ($<T_S$) for the measurement in FC protocol. The memory curve defined as $M^{\mathrm{mem}}_{\mathrm{FCH}}$ is depicted in Fig. 3(b) in addition to $M^{\mathrm{stop}}_{\mathrm{FCC}}$ and $M^{\mathrm{ref}}_{\mathrm{FCC}}$. Here, $M^{\mathrm{stop}}_{\mathrm{FCC}}$ is the FC curve recorded in cooling mode with two stops at 30 and 12 K, while $M^{\mathrm{ref}}_{\mathrm{FCC}}$ describes the same with continuous measurement considered as a reference curve for the comparison. A significant change in $M^{\mathrm{mem}}_{\mathrm{FCH}}$ is evident above 12 K which is missing around 30 K. This indicates that memory effect is sustained below $T_S$ and absent above $T_S$. Memory effect observed in FC protocol may appear due to extrinsic effect [29]. To test whether it occurs intrinsically, the memory experiment is performed in the ZFC protocol [30]. Similar to the experiment done in FC protocol, the sample is annealed at 12 K during the cooling process in zero field. The memory and reference curves described as $M^{\mathrm{mem}}_{\mathrm{ZFCH}}$ and $M^{\mathrm{ref}}_{\mathrm{ZFCH}}$, respectively, are depicted in Fig. 3(c). The difference between these curves described as $\Delta M$ is shown in the inset of the figure. The $\Delta M$ vs $T$ plot clearly shows a dip at 12 K and demonstrates the memory effect as commonly revealed for the SGs. In SG the spin-spin correlation length grows during the annealing process, even in zero field, and this is manifested through the memory dip. The development of spin-spin correlation length in zero field indicates the cooperative phenomenon as revealed for SG [31].

Time ($t$) dependence of $M(t)$ is recorded at 12 ($<T_S$) and 30 K ($>T_S$), at which experiment on memory effect is performed in FC mode. The sample is cooled in 100 Oe from well above $T_N$ down to desired temperatures and decay of $M(t)$ is recorded with $t$. Although signature of memory effect is absent at 30 K, a significant relaxation of $M(t)$ up to ∼2.5% is observed compared to ∼5.5% decay at 12 K for $t = 3000$ s as shown in Fig. 3(d). The $M(t)$ is fitted with the modified stretched exponential function, $M(t) = M_0 - M_g \exp[-(t/\tau)^{\beta}]$. The $M_0$ and $M_g$ are the ferromagnetic (FM) and exponential components of $M(t)$. $\beta$ is an exponent which lies in the range $0 < \beta \leqslant 1$. In the above expression, $\beta < 1$ indicates the relaxation mechanism involving activation against multiple anisotropy barriers as proposed for SGs. It may be noted that $M_0$ is required to fit the low-$t$ region of the $M(t) - t$ curve. Satisfactory fit using the above expression is displayed in Fig. 3(d) by the continuous curves. The values of $M_g/M_0$, $\tau$, and $\beta$ are 7.2%, 597 s, and 0.5, respectively, at 12 K and 3.2%, 804 s, and 0.42, respectively, at 30 K. The significantly large value of $M_0$ indicates the signature of dominant FM component in the relaxation dynamics, as observed in manganites [32] and alloy [28] displaying SG-like behavior. Here, $M_0$ appears due to coexistence of ferrimagnetic order associated with the glassy magnetic component. It is noteworthy that memory effect could not be detected at 30 K even in FC protocol, although a significant magnetization decay following glassy magnetic behavior is observed. This indicates that existence of SG like relaxation dynamics may not always lead to the memory effect even in FC protocol.

Dielectric permittivity ($\epsilon$) is measured at different $f$. The real ($\epsilon'$) and imaginary ($\epsilon''$) components of $\epsilon$ with $T$ are depicted in Fig. 4(a). The $\epsilon'(T)$ displays a significant decrease with decreasing temperature and it becomes nearly temperature independent below ∼150 K. Temperature dependent dielectricity above ∼150 K appears due to grain boundary effect. The $\epsilon'(T)$ and $\epsilon''(T)$ do not reveal any convincing signature of anomaly at $T_N$. Rather, a maximum in $\epsilon'(T)$ ($T_{FE}$) is observed close to $T_S$ suggesting a magnetoelectric coupling. The signature of $T_S$ is not convincingly observed

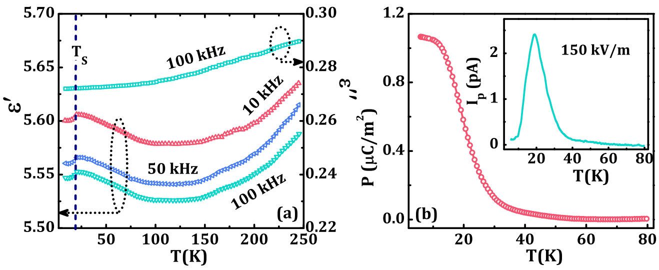

FIG. 4. (Color online) (a) Thermal variations of real part ($\epsilon'$) in left panel and imaginary part ($\epsilon''$) in right panel of dielectric permittivity at different $f$. (b) Electric polarization ($P$) with $T$. Inset of (b) shows pyroelectric current ($I_p$) with $T$.

in $\epsilon''(T)$. However, appearance of maximum or peak in $\epsilon'(T)$ indicates a fluctuation in electric polarization ($P$). The absence of $f$ dispersion as shown in Fig. 4(a) further points to the involvement of long-range ordering of electric polarization [33,34]. To confirm the origin of fluctuation of $P$, $I_p$ is recorded with $T$ in the warming mode. A sharp peak in $I_p(T)$ is observed as displayed in the inset of Fig. 4(b), at which the peak in $\epsilon'(T)$ is noticed. Time integrated $I_p$ provides $P$ as a function of $T$ which is depicted with $T$ in Fig. 4(b). Thus concomitant appearance of $T_{FE}$ and $T_S$ suggests that $MnCr_2O_4$ is a new member of improper multiferroics. The magnitude of $P$ ($\sim$1.08 $\mu$C/m$^2$) at 5 K for 150 kV/m poling field is significant among reported improper multiferroics [35–37].

The structural properties are thoroughly investigated by x-ray powder diffraction studies using a high flux synchrotron source over a wide temperature range, 10–300 K. Microstructural parameters are obtained from careful analysis of the diffraction patterns using Rietveld refinement. The refinement is done using $Fd\bar{3}m$ space group with atomic positions, Mn (0 0 0), Cr (0.625,0.625,0.625), and O ($x = y = z$) in the whole temperature range. This is consistent with the previous results proposing that magnetic $A$ site ion in $ACr_2O_4$ without orbital degeneracy usually maintains cubic symmetry even in the low temperature magnetic ground state [15,22,38]. Examples of the fits (continuous curves) with the experimental data (symbols) at 10 ($<T_S$) and 300 K ($\gg T_N$) are displayed in Figs. 5(a) and 5(b), respectively. The difference plot shown at the bottom of each plot confirms the single phase without trace amount of impurity. The reliability parameters $R_w(\sim 2.93)$, $R_{\text{expt}}(\sim 2.42)$, and $\chi^2(\sim 1.21)$ at 300 K and $R_w(\sim 3.08)$, $R_{\text{expt}}(\sim 2.32)$, and $\chi^2(\sim 1.33)$ at 10 K are reasonably small and close. This indicates that cubic structure with $Fd\bar{3}m$ space group holds even below the second magnetic transition at $T_S$.

In the thermal variation, the coordinate of O2 varies which is depicted in Fig. 5(c) as obtained from the refinement. The figure shows a steplike change close to $T_N$ and $T_S$. Thermal variation of lattice constant $a$ as obtained from the refinement is depicted in Fig. 5(d). An apparent signature of anomaly is evident at $T_N$ in the thermal variation. This clearly reveals a strong magnetoelastic coupling at $T_N$, although magnetoelastic coupling could not be detected in the dynamical properties of the lattice structure as probed by optical spectroscopy [39]. The synchrotron diffraction results further indicate that emergence of strong magnetoelastic coupling is not correlated with the orbital degeneracy of the $A$-site magnetic ion in $ACr_2O_4$ [39]. A change of slope in $a(T)$ is observed at $T_S$, also indicating the magnetoelastic coupling. This signature is more evident in Figs. 5(e)–5(j). Integrated intensity of (220) diffraction peak as indexed in Fig. 5(a) with $T$ is depicted in Fig. 5(e) which also displays clear signatures of $T_N$ and $T_S$. Signature of anomaly in the integrated intensity of (220) diffraction peak at $T_S$ may be correlated to the observed $T_{FE}$ and maximum in $\epsilon'$. This has also been observed in various systems [33,40].

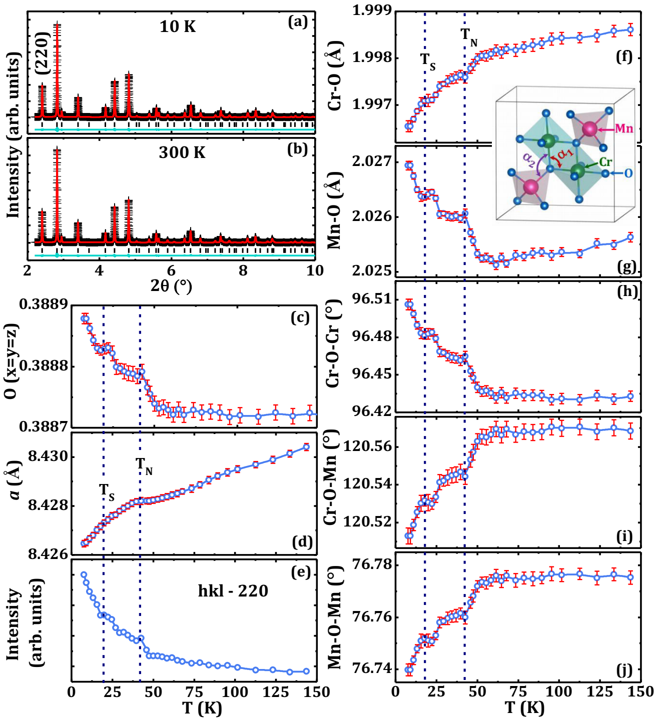

FIG. 5. (Color online) Rietveld refinement of x-ray powder diffraction patterns (black symbols) at 10 (a) and 300 K (b). Solid curves demonstrate the fits. $T$ variations of (c) positional coordinate of O2 [O($x = y = z$)], (d) $a$, and (e) normalized integrated intensities of (220) peak. $T$ variations of (f) Cr–O, (g) Mn–O bond lengths, and (h) Cr–O–Cr ($\alpha_1$), (i) Mn–O–Cr ($\alpha_2$), and (j) Mn–O–Mn ($\alpha_3$) bond angles. Inset of (f) and (g) shows Cr octahedra and Mn tetrahedra displaying bond lengths and bond angles.

As depicted in the inset of Figs. 5(f) and 5(g) $Mn^{2+}$ and $Cr^{3+}$ reside at the tetrahedral and octahedral sites, respectively, where corners of Mn tetrahedron and Cr octahedron are occupied by oxygen atoms. The Cr–O ($d_{\text{Cr–O}}$) and Mn–O ($d_{\text{Mn–O}}$) bond lengths, and Cr–O–Cr ($\alpha_1$) and Mn–O–Cr ($\alpha_2$) bond angles are depicted in the inset of the figures. Thermal variation of $d_{\text{Cr–O}}$, $d_{\text{Mn–O}}$, $\alpha_1$, $\alpha_2$, and Mn–O–Mn ($\alpha_3$) are shown in Figs. 5(f)–5(j). More convincing signatures of $T_N$ and $T_S$ are evident in the thermal variation of these microscopic structural parameters. In Fig. 5(f) the $d_{\text{Cr–O}}$ decreases with decreasing temperature and it shows steplike structures at both $T_N$ and $T_S$. The $d_{\text{Mn–O}}$ also decreases with decreasing temperature from 300 K and it shows anomalously significant rises with apparent steplike structures close to $T_N$ and $T_S$ as shown in Fig. 5(g). The anomalous increase of $d_{\text{Mn–O}} \sim 0.002$ Å from $\sim$50 K to $\sim$10 K is significant for an isostructural transition [33]. Thermal variations of bond lengths clearly demonstrate the contraction of $CrO_6$ octahedra and anomalous expansion of $MnO_4$ tetrahedra with decreasing temperature. This indicates that Cr–Cr superexchange interaction becomes stronger below $T_N$ than the Mn–Mn superexchange interaction. The oxygen displacement also leads to the significant changes in $\alpha_1$, $\alpha_2$, and $\alpha_3$ at $T_N$ and $T_S$ as displayed in Figs. 5(h), 5(i), and 5(j), respectively. Both $\alpha_1$ and $\alpha_2$ are nearly temperature independent with decreasing temperature up to $\sim$50 K, below which $\alpha_1$ increases quite sharply displaying steplike features at $T_N$ and $T_S$ in the temperature variation, whereas $\alpha_2$ and $\alpha_3$ decrease below $\sim$50 K with similar steplike features at $T_N$ and $T_S$ with decreasing temperature.

The x-ray diffraction studies reveal that occurrence of ferroelectricity does not involve any structural transition from centrosymmetric $Fd\bar{3}m$ space group to a noncentrosymmetric structure. Rather, diffraction studies demonstrate isotrructural

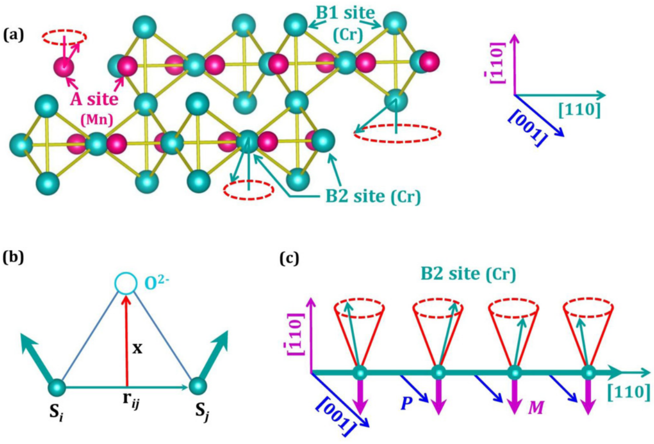

FIG. 6. (Color online) (a) Structure viewed along the conical spin modulation direction (110). The circles with inclined arrows indicate the spiral plane of the respective Mn, Cr($B1$), and Cr($B2$) spins with conical structure. (b) Possible direction of $O^{2-}$ ion displacement driven by DM interaction between $i$th ($\mathbf{S}_i$) and $j$th ($\mathbf{S}_j$) spins according to inverse DM model. (c) Directions of the net magnetization $\mathbf{M}$, the spiral spin modulation vector (110), and the induced polarization $\mathbf{P}$ for $B2$ site Cr chain.

transition with a discontinuous oxygen displacement at $T_N$ and $T_S$ analogous to that observed in $LiCrO_2$ [33]. Thus results clearly demonstrate that $MnCr_2O_4$ is an improper ferroelectric material where short-range spiral magnetic order gives rise to the ferroelectric order. The microscopic mechanism of occurrence of FE in magnetic spirals has been discussed in the literature which are correlated to the various spiral magnetic structures [22,36]. In Fig. 6(a) the structure as obtained from the neutron diffraction studies is shown along the conical spin modulation direction (110) for $MnCr_2O_4$ [7,14,15]. The circles with inclined arrows in Fig. 6(a) indicate the spiral plane of the respective spins with conical spin structures for Mn, $B1$, and $B2$ sites of Cr. The spiral magnetic order driven polarization may be understood in terms of the spin current model, $\mathbf{P} = \xi \mathbf{r}_{ij} \times \mathbf{S}_i \times \mathbf{S}_j$, where $\xi$ is the proportional constant as dependent on the spin exchange and spin-orbit interactions, and $\mathbf{r}_{ij}$ is a vector connecting $i$th and $j$th magnetic atoms. $\mathbf{S}_i$ and $\mathbf{S}_j$ are the spin vectors [41]. In case of the spin current model it has been suggested that the DM interaction induces ferroelectric polarization of the electronic orbitals without the involvement of the lattice degrees of freedom. Here, low temperature diffraction studies reveal isostructural discontinuous oxygen displacement at the onset of ferroelectric order and indicate that the spin-current model may not fit for interpreting the ferroelectricity in $MnCr_2O_4$.

Another alternative scenario of occurrence of $\mathbf{P}$ is driven by the inverse Dzyaloshinskii-Moriya (DM) interaction, where spiral magnetic order can polarize an oxygen (ligand) atom through the magnetostriction. The antisymmetric DM interaction is described as $\mathbf{D}_{ij} \cdot \mathbf{S}_i \times \mathbf{S}_j$ [42]. $\mathbf{D}_{ij} = \mathbf{x} \times \mathbf{r}_{ij}$ is the Dzyaloshinskii vector where $\mathbf{x}$ is perpendicular to $\mathbf{r}_{ij}$ as depicted in Fig. 6(b). Thus stronger DM interaction pushes oxygen atoms along the $\mathbf{x}$ direction. As depicted in Figs. 5(h)–5(j) $\alpha_1$ increases, whereas $\alpha_2$ and $\alpha_3$ decrease significantly below $T_S$. These results are correlated to the inverse DM interaction. We note from the changes of $\alpha$ values at $T_S$ that oxygen ions ($O^{2-}$) in Fig. 6(b) move toward $\mathbf{r}_{ij}$ for Cr–O–Cr superexchange path. On the other hand, oxygen moves away from $\mathbf{r}_{ij}$ for Mn–O–Cr and Mn–O–Mn superexchange paths. The conical spin modulation direction (110) for the $B2$ site of Cr, magnetization ($\mathbf{M}$), and $\mathbf{P}$ vectors are described in Fig. 6(c). The figure indicates possible polarization direction along (001) for $B2$ sites of Cr. In the case of inverse DM interaction the effect of the DM interaction is twofold; it induces the FE lattice displacements and stabilizes short-range spiral magnetic order at low temperature. The diffraction studies confirm the oxygen displacement involving ferroelectric order. The results further suggest that release of topological frustration and short-range spiral magnetic order are settled through the oxygen displacement.

Neutron diffraction studies confirmed appearance of long-range FIM order at $T_N$ followed by an emergence of another short-range spiral magnetic order below $T_S$ in $MnCr_2O_4$ [7,14,15]. The Cr atoms forming pyrochlore structure, as highlighted in Fig. 1, causes significant topological frustration. The interplay between ordering of $A$ site Mn moment and $B$ site Cr moment forming pyrochlore sublattice settles coexistence of SG-like and long-ranged FIM orders. Coexistence of SG-like component and long-range FIM order leads us to propose the reentrant SG (RSG) ground state. Thus topological frustration is the key for RSG state, spiral short-range order, and ferroelectricity in $MnCr_2O_4$.

In conclusion, the observed ferroelectricity is driven by spiral magnetic order, suggesting that $MnCr_2O_4$ is an improper ferroelectric material. Below spiral spin order zero-field-cooled memory effect and linear temperature dependence of magnetic entropy further suggest a reentrant spin-glass-like state. The significant magnetoelastic coupling is observed, which has been correlated to the release of topological frustration at $T_N$ and $T_S$.

## ACKNOWLEDGMENTS

S.G. acknowledges the financial support for experiment at DESY, Germany under DST-DESY project and DST for experiment at KEK, Tsukuba, Japan for synchrotron diffraction studies. S.G. wishes to thank Uta Rütt and O. Gutowski of HASYLAB, DESY, Germany and Sanjay Singh of Indian beam line at KEK, Japan for discussions and technical support during experiment. S.G. also acknowledges Nanoscience unit of IACS, Kolkata for the MPMS and TEM facilities. K.D. wishes to thank CSIR, India for support from a SRF fellowship.

---

[1] A. P. Ramirez, Annu. Rev. Mater. Sci. **24**, 453 (1994).
[2] S.-H. Lee, H. Takagi, D. Louca, M. Matsuda, S. Ji, H. Ueda, Y. Ueda, T. Katsufuji, J.-H. Chung, S. Park, S.-W. Cheong, and C. Broholm, J. Phys. Soc. Jpn. **79**, 011004 (2010).
[3] A. P. Ramirez, in *Handbook of Magnetic Materials*, edited by K. H. J. Buschow (Elsevier, Amsterdam, 2001), Vol. 13, p. 423.
[4] H. Ueda, H. Mitamura, T. Goto, and Y. Ueda, Phys. Rev. B **73**, 094415 (2006).

[5] H. Ueda, H. A. Katori, H. Mitamura, T. Goto, and H. Takagi, Phys. Rev. Lett. **94**, 047202 (2005).

[6] S.-H. Lee, C. Broholm, T. H. Kim, W. Ratcliff, and S.-W. Cheong, Phys. Rev. Lett. **84**, 3718 (2000).

[7] K. Tomiyasu, J. Fukunaga, and H. Suzuki, Phys. Rev. B **70**, 214434 (2004).

[8] E. Winkler, S. Blanco Canosa, F. Rivadulla, M. A. López-Quintela, J. Rivas, A. Caneiro, M. T. Causa, and M. Tovar, Phys. Rev. B **80**, 104418 (2009).

[9] M. R. Suchomel, D. P. Shoemaker, L. Ribaud, M. C. Kemei, and R. Seshadri, Phys. Rev. B **86**, 054406 (2012); T. D. Sparks, M. C. Kemei, P. T. Barton, R. Seshadri, E.-D. Mun, and V. S. Zapf, *ibid.* **89**, 024405 (2014).

[10] R. N. Bhowmik, R. Ranganathan, and R. Nagarajan, Phys. Rev. B **73**, 144413 (2006).

[11] K. Ohgushi, Y. Kokimoto, T. Ogasawara, S. Miyasaka, and Y. Tokura, J. Phys. Soc. Jpn. **77**, 034713 (2008).

[12] N. Mufti, G. R. Blake, and T. T. M. Palstra, J. Magn. Magn. Mater. **321**, 1767 (2009).

[13] Y. H. Zhou, Z. R. Yang, L. Li, Y. M. Xie, S. Lin, Y. P. Sun, and Y. H. Zhang, J. Magn. Magn. Mater. **324**, 3799 (2012).

[14] R. Plumier, J. Appl. Phys. **39**, 635 (1968).

[15] J. M. Hastings and L. M. Corliss, Phys. Rev. **126**, 556 (1962).

[16] D. Y. Yoon, S. Lee, Y. S. Oh, and K. H. Kim, Phys. Rev. B **82**, 094448 (2010).

[17] C. Ederer and M. Komelj, Phys. Rev. B **76**, 064409 (2007).

[18] M. Matsubara, Y. Shimada, K. Ohgushi, T. Arima, and Y. Tokura, Phys. Rev. B **79**, 180407(R) (2009).

[19] N. Mufti, A. A. Nugroho, G. R. Blake, and T. T. M. Palstra, J. Phys.: Condens. Matter **22**, 075902 (2010).

[20] Y. Tokunaga, D. Okuyama, T. Kurumaji, T. Arima, H. Nakao, Y. Murakami, Y. Taguchi, and Y. Tokura, Phys. Rev. B **84**, 060406(R) (2011).

[21] G. Lawes, A. B. Harris, T. Kimura, N. Rogado, R. J. Cava, A. Aharony, O. Entin-Wohlman, T. Yildrim, M. Kenzelmann, C. Broholm, and A. P. Ramirez, Phys. Rev. Lett. **95**, 087205 (2005).

[22] Y. Yamasaki, S. Miyasaka, Y. Kaneko, J.-P. He, T. Arima, and Y. Tokura, Phys. Rev. Lett. **96**, 207204 (2006).

[23] M. Patra, K. De, S. Majumdar, and S. Giri, Appl. Phys. Lett. **94**, 092506 (2009).

[24] S. Klemme and M. Ahrens, Phys. Chem. Minerals **34**, 59 (2007).

[25] D. Meschede, F. Steglich, W. Felsch, H. Maletta, and W. Zinn, Phys. Rev. Lett. **44**, 102 (1980).

[26] D. L. Martin, Phys. Rev. B **20**, 368 (1979).

[27] D. De, A. Karmakar, M. K. Bhunia, A. Bhaumik, S. Majumdar, and S. Giri, J. Appl. Phys. **111**, 033919 (2012).

[28] A. Bhattacharyya, S. Giri, and S. Majumdar, Phys. Rev B **83**, 134427 (2011).

[29] Y. Sun, M. B. Salamon, K. Garnier, and R. S. Averback, Phys. Rev. Lett. **91**, 167206 (2003).

[30] M. Sasaki, P. E. Jönsson, H. Takayama, and P. Nordblad, Phys. Rev. Lett. **93**, 139701 (2004); R. K. Zheng, H. Gu, and X. X. Zhang, *ibid.* **93**, 139702 (2004).

[31] J. A. Mydosh, *Spin Glasses: An Experimental Introduction* (Taylor & Francis, London, 1993).

[32] K. De, M. Patra, S. Majumdar, and S. Giri, J. Phys. D: Appl. Phys. **40**, 7614 (2007).

[33] K. Dey, A. Karmakar, S. Majumdar, and S. Giri, Phys. Rev. B **87**, 094403 (2013).

[34] A. Karmakar, K. Dey, S. Chatterjee, S. Majumdar, and S. Giri, Appl. Phys. Lett. **104**, 052906 (2014).

[35] W. Eerenstein, N. D. Mathur, and J. F. Scott, Nature (London) **442**, 759 (2006).

[36] S.-W. Cheong and M. Mostovoy, Nat. Mater. **6**, 13 (2007).

[37] K. F. Wang, J.-M. Liu, and Z. F. Ren, Adv. Phys. **58**, 321 (2009).

[38] S. Bordács, D. Varjas, I. Kézsmárki, G. Mihály, L. Baldassarre, A. Abouelsayed, C. A. Kuntscher, K. Ohgushi, and Y. Tokura, Phys. Rev. Lett. **103**, 077205 (2009).

[39] V. Kocsis, S. Bordács, D. Varjas, K. Penc, A. Abouelsayed, C. A. Kuntscher, K. Ohgushi, Y. Tokura, and I. Kézsmárki, Phys. Rev. B **87**, 064416 (2013).

[40] K. Dey, A. Karmakar, S. Majumdar, and S. Giri, Scr. Mater. **75**, 94 (2014).

[41] H. Katsura, N. Nagaosa, and A. V. Balatsky, Phys. Rev. Lett. **95**, 057205 (2005).

[42] I. A. Sergienko and E. Dagotto, Phys. Rev. B **73**, 094434 (2006).